



Cite this: RSC Adv., 2018, 8, 13984

Received 19th March 2018  
 Accepted 10th April 2018

DOI: 10.1039/c8ra02390e  
[rsc.li/rsc-advances](http://rsc.li/rsc-advances)

## 1. Introduction

Heteropoly acids (HPAs) are a unique class of nanosized poly-nuclear clusters composed of transition metals and oxygen atoms.<sup>1,2</sup> During the past decades, HPAs have attracted huge interest owing to their huge potential in many fields, for instance, catalysts, biomedicine and material science.<sup>3–7</sup> In particular, due to their high proton conductivity and proton transfer/storage abilities, HPAs have become one of the best candidate electrolyte materials for the development of fuel cells and supercapacitors.<sup>8–12</sup> So, a further investigation of the role and function of these compounds in electrochemical devices will give insight into developing solid electrolytes based on HPAs.<sup>13</sup> HPAs contain two kinds of protons: (1) dissociated hydrated protons connected to one heteropolyanion as a whole; (2) non-hydrated protons located on the bridge-oxygen or terminal-oxygen atoms of the polyanion.<sup>14</sup>

Keggin-type HPAs, which are an important branch of HPAs, occupy an unique place at the forefront of the HPAs field because of their many advantages, including chemical stability and convenience of synthesis.<sup>15,16</sup> Its chemical formula can be expressed as  $[XM_{12}O_{40}]^{n-}$ , with mainly X = P, As, Si and Ge, and M = W, Mo and V. What attracts us most is that the structure and proton conductive property of HPAs vary with the component elements of heteropolyanion changes. According to our recent researches,<sup>17</sup> vanadium have great impact on the thermal stability and proton conductivity of heteropoly acids. Hence, in this work, based on Keggin-type HPAs, a mono-vanadium-substituted molybdo vanadosilicic acid  $H_5SiMo_{11}VO_{40} \cdot 8H_2O$  is synthesized,

## Synthesis and performance of solid proton conductor molybdo vanadosilicic acid

Zhirong Xie,<sup>a</sup> Han Wu,<sup>a</sup> Qingyin Wu<sup>\*a</sup> and Limei Ai<sup>b</sup>

A molybdo vanadosilicic acid  $H_5SiMo_{11}VO_{40} \cdot 8H_2O$  was synthesized and investigated in this work. The structure features and hydration degree of this acid were characterized by IR, UV, XRD and TG-DTA. Its proton conductivity was studied by electrochemical impedance spectroscopy (EIS). The EIS measurements demonstrated that  $H_5SiMo_{11}VO_{40} \cdot 8H_2O$  showed excellent proton conduction performance with proton conductivity reaching  $5.70 \times 10^{-3} \text{ S cm}^{-1}$  at 26 °C and 70% relative humidity. So, it is a new solid high proton conductor. The conductivity enhances with the increase of temperature, and it exhibits Arrhenius behavior. The activation energy value for proton conduction is 21.4 kJ mol<sup>-1</sup>, suggesting that the proton transfer in this solid acid is dominated by Vehicle mechanism.

and its structure, hydration and proton conductive properties have also been investigated.

## 2. Experimental section

### 2.1. Preparation of $H_5SiMo_{11}VO_{40} \cdot 8H_2O$

2.84 g of  $Na_2SiO_3 \cdot 9H_2O$  was dissolved in 100 mL deionized water, and added 26.62 g  $Na_2MoO_4 \cdot 2H_2O$  to the above solution. Then this mixed solution was heated to boil for 30 min. After that, 50 mL aqueous solution which contained 1.22 g  $NaVO_3$  was added to the mixture. The mixture was continuously heated at 90 °C for 2 h with the assistance of stirring under the condition of pH = 2.5 (adjusted by 1 : 1  $H_2SO_4$  solution). Lastly, the cooled solution was extracted with 30 mL ether in sulfuric acid environment. The powder  $H_5SiMo_{11}VO_{40} \cdot 8H_2O$  was obtained after the concentrated etherate solution was dried in vacuum. The color of the product is orange-red and the morphology of this solid is as shown in Fig. 1, which indicates that this heteropoly acid exhibits crystalline structure. The element contents of silicon, molybdenum and vanadium in  $H_5SiMo_{11}VO_{40} \cdot 8H_2O$  were collected by inductively coupled plasma mass spectrometer (ICP-MS). The content of water was figured out by thermogravimetry. Found: Si: 1.37%; Mo: 54.06%; V: 2.49% and  $H_2O$ : 9.30%. Calculated for  $H_5SiMo_{11}VO_{40} \cdot 8H_2O$ : Si: 1.43%; Mo: 53.87%; V: 2.60% and  $H_2O$ : 9.18%. The theoretical values are in good agreement with the experimental results.

### 2.2. Instructions and reagents

Element content was measured on a THERMO ELECTRON PQ3 inductively coupled plasma mass spectrometer (ICP-MS). The Fourier-transform infrared spectroscopy (FTIR) spectrum was performed on a NICOLET NEXUS470 FT/IR spectrometer using

<sup>a</sup>Department of Chemistry, Zhejiang University, Hangzhou, 310027, P. R. China.  
 E-mail: qywu@zju.edu.cn

<sup>b</sup>School of Biomedical and Chemical Engineering, Liaoning Institute of Science and Technology, Benxi 117004, Liaoning, P. R. China



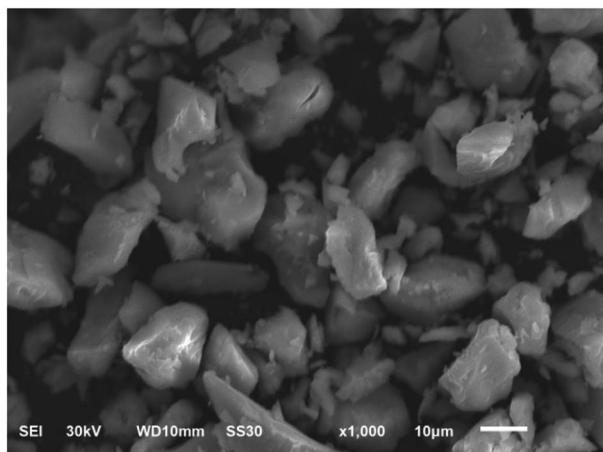


Fig. 1 The SEM of  $\text{H}_5\text{SiMo}_{11}\text{VO}_{40} \cdot 8\text{H}_2\text{O}$ .

KBr as pellets, and the resolution is  $4\text{ cm}^{-1}$ . UV spectrum was got using SHIMADZU UV-2550 UV-Vis spectrophotometer.

Powder X-ray diffraction (XRD) pattern was recorded on a BRUKER D8 ADVANCE X-ray diffractometer in the range of  $2\theta = 3\text{--}40^\circ$  at the rate of  $0.02^\circ\text{ s}^{-1}$ . The crystal data was collected using graphitemono-chromatic Mo-K radiation ( $0.71073\text{ \AA}$ ) at  $293\text{ K}$ , and the data sets were corrected by empirical absorption correction using spherical harmonics, implemented in SCALE3 ABSPACK scaling algorithm. The thermal stability of the sample was carried out using simultaneous thermogravimetry (TG) and differential thermal analysis (DTA) technique, measurements were performed using a Shimadzu thermal analyzer in a nitrogen stream from room temperature to  $600\text{ }^\circ\text{C}$ , with the scanning rate of  $10\text{ }^\circ\text{C min}^{-1}$ .

All chemicals were of analytical grade and used without further purification.

### 2.3. Measurement of proton conductivity

At ambient condition, the crushed sample was pressed at  $25\text{ MPa}$  into a compacted pellet. The diameter of the obtained tablet is  $10.00\text{ mm}$  and the thickness of it is  $1.02\text{ mm}$ . The proton conductivity was measured using a cell: copper | sample | copper, in which copper slices were attached to the two sides of the tablet as electrodes. Complex impedance measurements were carried out on a VMP2 multichannel potentiostat electrochemical impedance analyzer over a frequency range from  $9.99 \times 10^4$  to  $0.01\text{ Hz}$ .

## 3. Results and discussion

IR is a useful method for investigating the structure information of heteropoly compounds. There are four kinds of oxygen atoms in  $[\text{SiM}_{12}\text{O}_{40}]^{n-}$ . The  $\text{SiO}_4$  tetrahedron is located in the center of the twelve  $\text{MO}_6$  octahedra, which can be split into four groups of three edge-shared octahedra,  $\text{M}_3\text{O}_{13}$ . Furthermore, the  $\text{M}_3\text{O}_{13}$  units are connected together by shared corners to each other. So, there are four kinds of oxygen atoms in  $[\text{SiM}_{12}\text{O}_{40}]^{n-}$ :  $\text{Si}-\text{O}_a$ ,  $\text{M}-\text{O}_b-\text{M}$ ,  $\text{M}-\text{O}_c-\text{M}$  and  $\text{M}-\text{O}_d$ , where each separately represent inner oxygen, corner-sharing oxygen, edge-sharing oxygen and terminal

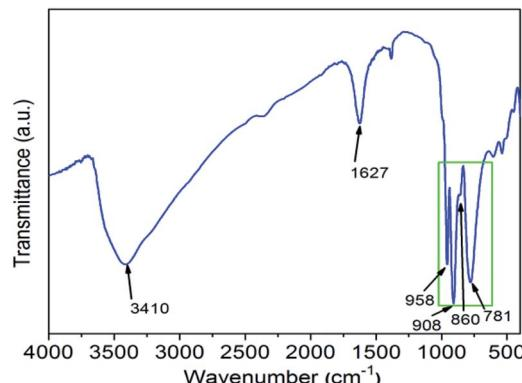


Fig. 2 The IR spectrum of  $\text{H}_5\text{SiMo}_{11}\text{VO}_{40} \cdot 8\text{H}_2\text{O}$ .

oxygen. Fig. 2 presents that, at the range of  $700\text{--}1000\text{ cm}^{-1}$ , the IR spectrum of  $\text{H}_5\text{SiMo}_{11}\text{VO}_{40} \cdot 8\text{H}_2\text{O}$  exhibits four characteristic peaks. They are  $958\text{ cm}^{-1}$ ,  $908\text{ cm}^{-1}$ ,  $860\text{ cm}^{-1}$  and  $781\text{ cm}^{-1}$ , which are assigned to  $\nu_{\text{as}}(\text{M}-\text{O}_d)$ ,  $\nu_{\text{as}}(\text{Si}-\text{O}_a)$ ,  $\nu_{\text{as}}(\text{M}-\text{O}_b-\text{M})$  and  $\nu_{\text{as}}(\text{M}-\text{O}_c-\text{M})$  vibration modes of heteropolyanion  $\text{SiMo}_{11}\text{VO}_{40}^{5-}$ . For comparison, these four peaks of  $\text{H}_4\text{SiMo}_{12}\text{O}_{40}$  are  $957\text{ cm}^{-1}$ ,  $904\text{ cm}^{-1}$ ,  $855\text{ cm}^{-1}$ ,  $770\text{ cm}^{-1}$ .<sup>18</sup> The similarity of vibration bands demonstrates that the heteropoly acid  $\text{H}_5\text{SiMo}_{11}\text{VO}_{40}$  has the Keggin structure as its parent acid  $\text{H}_4\text{SiMo}_{12}\text{O}_{40}$  does.<sup>19</sup> Obviously, all of these peaks have slightly shifted, which caused by the more negative charge carrier and the shift symmetry of molecular structure of  $\text{H}_5\text{SiMo}_{11}\text{VO}_{40} \cdot 8\text{H}_2\text{O}$ . Furthermore, there are two strong absorption peaks at  $3410\text{ cm}^{-1}$  and  $1627\text{ cm}^{-1}$  ascribed to the stretching vibration of O-H bond and the bending vibration of H-O-H bond.

The UV spectrum is very useful to distinguish the electronic properties of the metal ions. As shown in Fig. 3, there are three absorption bands identified in the UV spectrum of  $\text{H}_5\text{SiMo}_{11}\text{VO}_{40} \cdot 8\text{H}_2\text{O}$ . The intense peak at  $207\text{ nm}$  belongs to the charge-transfer from terminal oxygen to metal atoms ( $\text{O}_d \rightarrow \text{M}$ ). The relatively weak bands at  $247\text{ nm}$  and  $306\text{ nm}$  are ascribed to the charge-transfer from bridge oxygen to metal atoms ( $\text{O}_b/\text{O}_c \rightarrow \text{M}$ ). Inspired by the related literature,<sup>20</sup> we could conclude that these

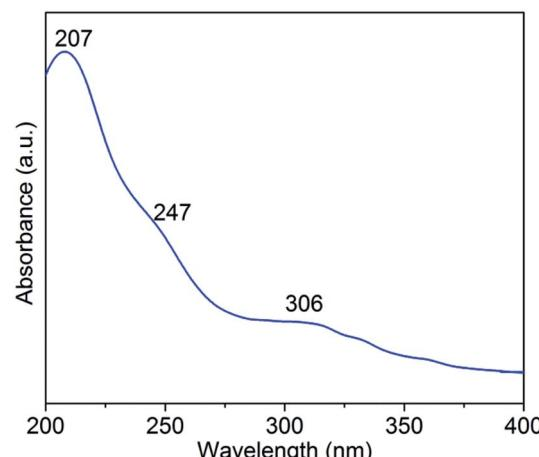


Fig. 3 The UV spectrum of  $\text{H}_5\text{SiMo}_{11}\text{VO}_{40} \cdot 8\text{H}_2\text{O}$ .

absorption bands are the characteristic bands of Keggin-type heteropolyanion.

We have also got some information about crystal structure of  $H_5SiMo_{11}VO_{40} \cdot 8H_2O$  by powder X-ray diffraction (XRD). Fig. 4 is the powder X-ray diffraction pattern of  $H_5SiMo_{11}VO_{40} \cdot 8H_2O$ . From the data of XRD in Table 1, we get to know that the characteristic peaks of this HPA mainly exist at the range of 8–10°, 17–23°, 25–32° and 33–38°, and the most intensive peak is at about 9.25°. They are the characteristic peaks of HPAs with Keggin structure.<sup>21</sup> Up to now, XRD, combined with UV and IR spectra, allows us to verify that the heteropoly acid  $H_5SiMo_{11}VO_{40}$  possesses the typical Keggin structure as shown in Fig. 5.

The hydration degree and thermal stability of  $H_5SiMo_{11}VO_{40} \cdot 8H_2O$  was investigated by thermogravimetric (TG) and differential thermal analysis (DTA). Generally, heteropoly acids contain three kinds of crystallographic water: crystal water, protonized water and structure water. As illustrated in Fig. 6, The TG curve shows the total percent of the weight loss below 383 °C is 9.30%, which indicates that 10.5 molecules of water calculated are lost. Firstly, the loss of 4.9 molecules crystal water happen with corresponding to the weight loss of 4.61%, then,

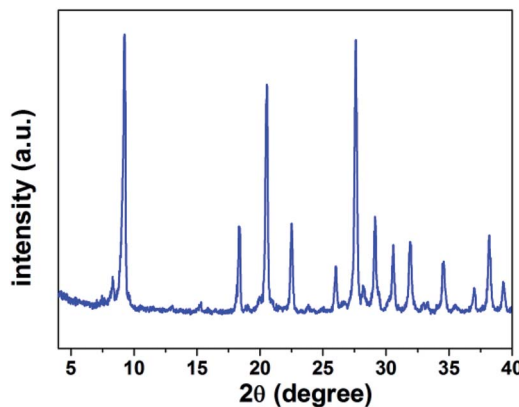


Fig. 4 The XRD pattern of  $H_5SiMo_{11}VO_{40} \cdot 8H_2O$ .

Table 1 Data of X-ray powder diffraction of  $H_5Mo_{11}VO_{40} \cdot 8H_2O$

$2\theta$	$I/I_0$	$d^a$ (Å)
9.25	1.00	9.55
18.33	0.32	4.83
20.67	0.81	4.29
22.49	0.32	3.95
25.93	0.18	3.43
27.63	0.97	3.22
29.10	0.34	3.06
30.43	0.25	2.93
31.90	0.26	2.80
34.58	0.19	2.59
36.93	0.09	2.43
38.17	0.28	2.35
39.27	0.11	2.29

<sup>a</sup>  $d$  represents the lattice plane spacing calculated according to Bragg equation:  $2d \sin \theta = n\lambda$ . ( $\lambda = 1.541$  Å for Cu-K $\alpha$ ).

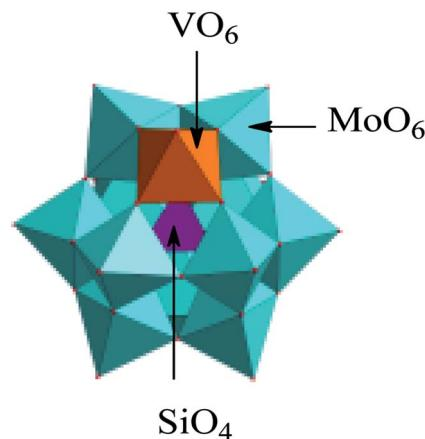


Fig. 5 The structure of heteropolyanion  $SiMo_{11}VO_{40}^{5-}$ . Color legend:  $VO_6$ , orange octahedra;  $MoO_6$ , green octahedra;  $SiO_4$ , purple tetrahedra.

4.1 molecules of protonized water are lost, and 1.4 molecules of crystal water are lost at last. Therefore, the accurate molecule formula of this heteropoly acid is  $(H_5O_2^+)_2H_3[SiMo_{11}VO_{40}] \cdot 5H_2O$ . What's more, it is noticed that there are two obvious peaks in DTA curve. The endothermic peak observed at 90 °C is believed to be the processes of the dehydration, and exothermic peak of 383 °C is attributed to the irreversible decomposition of heteropoly acid to individual oxides ( $SiO_2$ ,  $MoO_3$  and  $V_2O_5$ ). It demonstrates that the decomposition temperature of  $H_5SiMo_{11}VO_{40} \cdot 8H_2O$  is 383 °C. According to the reported literature,<sup>22,23</sup> the decomposition temperature of  $H_4SiMo_{12}O_{40} \cdot 2H_2O$  is 365 °C, indicating vanadium-containing heteropolyanion has better thermal stability than its parent acid.

The proton conductivity is one of the most important properties of heteropoly acids. Fig. 7 is the electrochemical impedance spectrum of  $H_5SiMo_{11}VO_{40} \cdot 8H_2O$ , and inset is the equivalent circuit, where  $R_1$  is the bulk resistance,  $C_1$  represents a constant phase element of the double layers,  $R_2$  denotes the charge transfer resistance and  $W_1$  is the finite length Warburg element of solid diffusion. The proton conductivity of HPA is calculated using the following equation:  $\sigma = L/(RS)$  ( $R$  is the resistance,  $L$  is the thickness, and  $S$  is the area of the tablet). By calculation, the proton conductivity of  $H_5SiMo_{11}VO_{40} \cdot 8H_2O$  is

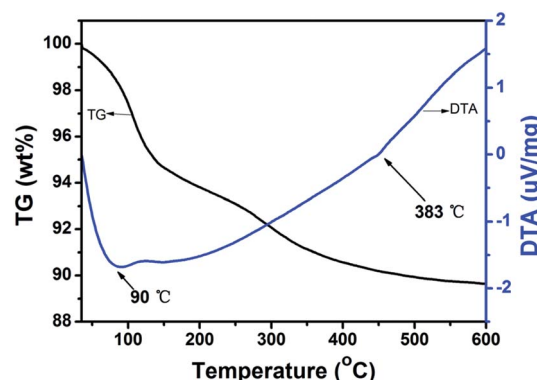


Fig. 6 The TG-DTA curves of  $H_5SiMo_{11}VO_{40} \cdot 8H_2O$ .



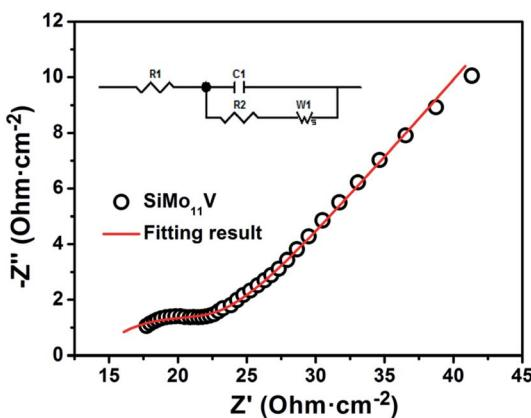


Fig. 7 The electrochemical impedance spectrum of  $\text{H}_5\text{SiMo}_{11}\text{VO}_{40}\cdot 8\text{H}_2\text{O}$  at 26 °C and 70% relative humidity.

$5.70 \times 10^{-3} \text{ S cm}^{-1}$  at 26 °C and 70% relative humidity. It shows a higher conductivity than  $\text{H}_4\text{SiMo}_{12}\text{O}_{40}\cdot 12\text{H}_2\text{O}$  ( $2.03 \times 10^{-4} \text{ S cm}^{-1}$ ),<sup>24</sup> which illustrated that the incorporation of V element can increase hugely the proton conductivity of silicomolybdic acid. So, this heteropoly compound is a high proton conductor. Additionally, CPE for double layers from the equivalent circuit is  $3.59 \times 10^{-3} \text{ F}$ , indicating that this acid has the potential for application in energy storage device, such as supercapacitors.

To investigate the relationship between proton conductivity and temperature, we measured the conductivity of this heteropoly acid at the temperature range of 26–60 °C. It is found that the conductivity value of this heteropoly acid enhances with higher temperature because the mobility of conducting species accelerates with the increase of temperature, which increases to  $1.35 \times 10^{-2} \text{ S cm}^{-1}$  at 60 °C and 70% relative humidity. The relationship between proton conductivity and temperature is consistent with Arrhenius equation:  $\sigma = \sigma_0 \exp^{(E_a/kT)}$ . In this formula,  $E_a$  is the activation energy of proton conductivity,  $\sigma_0$  is the pre-exponential factor and  $k$  presents the Boltzmann constant. As shown in Fig. 8, the activation energy of proton conductivity calculated from the slope of Arrhenius curve is  $21.4 \text{ kJ mol}^{-1}$ .

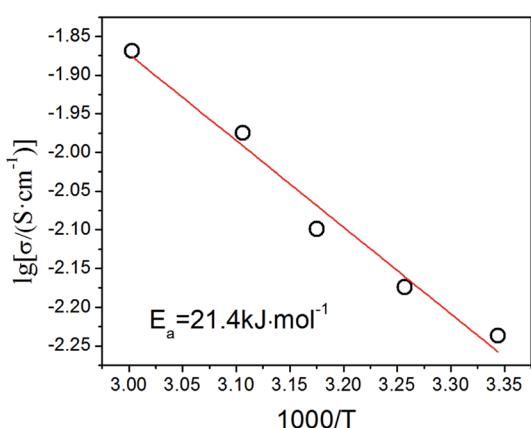


Fig. 8 The Arrhenius plot for conductivity of  $\text{H}_5\text{SiMo}_{11}\text{VO}_{40}\cdot 8\text{H}_2\text{O}$ .

So far, there are two major recognized proton conduction mechanisms: Vehicle and Grotthuss mechanism.<sup>25,26</sup> In Vehicle mechanism, proton interacts with water molecules, which transfers in the form of hydrated hydrogen ions, such as  $\text{H}_3\text{O}^+$ ,  $\text{H}_5\text{O}_2^+$  and  $\text{H}_9\text{O}_4^+$  species, similar to molecular diffusion. It differs from Grotthuss mechanism, in which a large amount of water can assist proton hopping from one proton carrier to a neighboring one down a chain of hydrogen-bonded network. Therefore, water plays a fairly important role in the process of proton mobility, and proton conductivity and Arrhenius parameters are strongly dependent on the water content.<sup>27,28</sup> Generally, we distinguish them by the numerical value of activation energy and the type of hydrated hydrogen ions. The activation energy of Grotthuss mechanism is often less than  $15 \text{ kJ mol}^{-1}$ , which is lower than that of Vehicle mechanism, whose is normally more than  $20 \text{ kJ mol}^{-1}$ .<sup>29,30</sup> The activation energy of this acid is  $21.4 \text{ kJ mol}^{-1}$ . The acid protons and water molecules form  $\text{H}_5\text{O}_2^+$  that bridges the Keggin units owing to the low hydration levels (less than 10 water molecules of hydration per Keggin unit).<sup>31</sup> Hence, we can speculate that the proton migration of  $\text{H}_5\text{SiMo}_{11}\text{VO}_{40}\cdot 8\text{H}_2\text{O}$  occurs by a mixing mechanism and Vehicle mechanism is predominant.

## 4. Conclusions

In this work, we have reported the synthesis of a vanadium-substituted heteropoly acid  $\text{H}_5\text{SiMo}_{11}\text{VO}_{40}\cdot 8\text{H}_2\text{O}$ , which was characterized by IR, XRD of powder, TG-DTA. This acid shows a good proton conductivity of  $5.70 \times 10^{-3} \text{ S cm}^{-1}$  at 26 °C and 70% relative humidity. The proton conductivity enhances with the increase of temperature, and the proton conduction mechanism is dominated by Vehicle mechanism due to the activation energy of  $21.4 \text{ kJ mol}^{-1}$ . It is a novel solid high proton conductor, which may be applied as solid electrolyte in the fields of fuel cell and supercapacitors.

## Conflicts of interest

There are no conflicts to declare.

## Acknowledgements

This work is financially supported by the National Key Research and Development Program of China (2016YFB0901600), the Zhejiang Provincial Natural Science Foundation of China (LY18B010001), the Liaoning Provincial Natural Science Foundation of China (201602404) and the Scientific Research Foundation of Liaoning Institute of Science and Technology (RXYJ2015001).

## References

- 1 M. Shiddiq, D. Komijani, Y. Duan, A. Gaita-Ariño, E. Coronado and S. Hill, *Nature*, 2016, **531**, 348–351.
- 2 C. Zhang, W. B. Bu, D. L. Ni, C. J. Zuo, C. Cheng, Q. Li, L. L. Zhang, Z. Wang and J. L. Shi, *J. Am. Chem. Soc.*, 2016, **138**, 8156–8164.



- 3 Y. W. Liu, S. M. Liu, X. Y. Lai, J. Miao, D. F. He, N. Li, F. Luo, Z. Shi and S. X. Liu, *Adv. Funct. Mater.*, 2015, **25**, 4480–4485.
- 4 J. J. Chen, M. D. Symes, S. C. Fan, M. S. Zheng, H. N. Miras, Q. F. Dong and L. Cronin, *Adv. Mater.*, 2017, **27**, 4649–4654.
- 5 A. Rubinstein, P. Jiménez-Lozanao, J. J. Carbó, J. M. Poblet and R. Neumann, *J. Am. Chem. Soc.*, 2014, **136**, 10941–10948.
- 6 T. Yoshida, T. Murayama, N. Sakaguchi, M. Okumura, T. Ishida and M. Haruta, *Angew. Chem., Int. Ed.*, 2018, **57**, 1523–1527.
- 7 X. F. Wu, W. Wu, Q. Y. Wu and W. F. Yan, *Langmuir*, 2017, **33**, 4242–4249.
- 8 M. Tountas, Y. Topal, A. Verykios, A. Soultati, A. Kaltzoglou, T. A. Papadopoulos, F. Auras, K. Seintis, M. Fakis, L. C. Palilis, D. Tsikritzis, S. Kennou, A. Fakharuddin, L. Schmidt-Mende, S. Gardelis, M. Kus, P. Falaras, D. Davazoglou, P. Argitis and M. Vasilopoulou, *J. Mater. Chem. C*, 2018, **6**, 1459–1469.
- 9 M. H. Yang, B. G. Choi, S. C. Jung, Y. K. Han, Y. S. Huh and S. B. Lee, *Adv. Funct. Mater.*, 2014, **24**, 7301–7309.
- 10 J. J. Chen, J. C. Ye, X. G. Zhang, M. D. Symes, S. C. Fan, D. L. Long, M. S. Zheng, D. Y. Wu, L. Cronin and Q. F. Dong, *Adv. Energy Mater.*, 2018, **8**, 1701021.
- 11 H. Gao, A. Virya and K. Lian, *J. Mater. Chem. A*, 2015, **3**, 21511–21517.
- 12 X. Tong, N. Q. Tian, W. Wu, W. M. Zhu, Q. Y. Wu, F. H. Cao, W. F. Yan and A. B. Yaroslavtsev, *J. Phys. Chem. C*, 2013, **117**, 3258–3263.
- 13 X. F. Wu, X. Tong, Q. Y. Wu, H. Ding and W. F. Yan, *J. Mater. Chem. A*, 2014, **2**, 5780–5784.
- 14 U. Thanganathan, *J. Mater. Chem.*, 2011, **21**, 456–465.
- 15 Y. Leng, J. Wang, D. R. Zhu, X. Q. Ren, H. Q. Ge and L. Shen, *Angew. Chem., Int. Ed.*, 2009, **48**, 168–171.
- 16 H. Miao, X. Xu, W. W. Ju, H. X. Wan, Y. Zhang, D. R. Zhu and Y. Xu, *Inorg. Chem.*, 2014, **53**, 2757–2759.
- 17 T. P. Huang, N. Q. Tian, Q. Y. Wu, Y. Yan and W. F. Yan, *Mater. Chem. Phys.*, 2015, **165**, 34–38.
- 18 C. Rocchiccioli-Deltcheff, M. Fournier, R. Franck and R. Thouvenot, *Inorg. Chem.*, 1983, **22**, 207–216.
- 19 Y. Leng, J. Wang, D. R. Zhu, Y. J. Wu and P. P. Zhao, *J. Mol. Catal. A: Chem.*, 2009, **313**, 1–6.
- 20 Y. Ding, Q. Gao, G. X. Li, H. P. Zhang, J. M. Wang, L. Yan and J. S. Suo, *J. Mol. Catal. A: Chem.*, 2004, **218**, 161–170.
- 21 Y. P. Wang, B. B. Zhou and L. H. Zhang, *J. Alloys Compd.*, 2014, **601**, 126–129.
- 22 X. E. Cai, D. C. Du, J. P. Ni, Y. M. Jin, J. Zhu and Y. X. Qian, *Thermochim. Acta*, 1997, **292**, 45–50.
- 23 Y. Y. Li, X. F. Wu, Q. Y. Wu, H. Ding and W. F. Yan, *Ind. Eng. Chem. Res.*, 2014, **53**, 12920–12926.
- 24 Q. Y. Wu and G. Y. Meng, *Mater. Res. Bull.*, 2000, **35**, 85–91.
- 25 K. D. Kreuer, W. Weppner and A. Rabenau, *Angew. Chem., Int. Ed.*, 1982, **21**, 208–209.
- 26 T. Dippel, K. D. Kreuer, J. C. Lassegues and D. Rodriguez, *Solid State Ionics*, 1993, **61**, 41–46.
- 27 E. Jaimez, G. B. Hix and R. C. T. Slade, *J. Mater. Chem.*, 1997, **7**, 475–479.
- 28 R. C. T. Slade, G. P. Hall, A. Ramanan and E. Prince, *Solid State Ionics*, 1996, **92**, 171–181.
- 29 K. Checkiewicz, G. Zukowska and W. Wieczorek, *Chem. Mater.*, 2001, **13**, 379–384.
- 30 A. Eguizabal, J. Lemus, M. Urbiztundo, O. Garridob, J. Solera, J. A. Blazquezb and M. P. Pinaa, *J. Power Sources*, 2011, **196**, 8994–9007.
- 31 D. I. Kolokolov, M. S. Kazantsev, M. V. Luzgin, H. Jobic and A. G. Stepanov, *J. Phys. Chem. C*, 2014, **118**, 30023–30033.